CHAPTER 1

Introduction

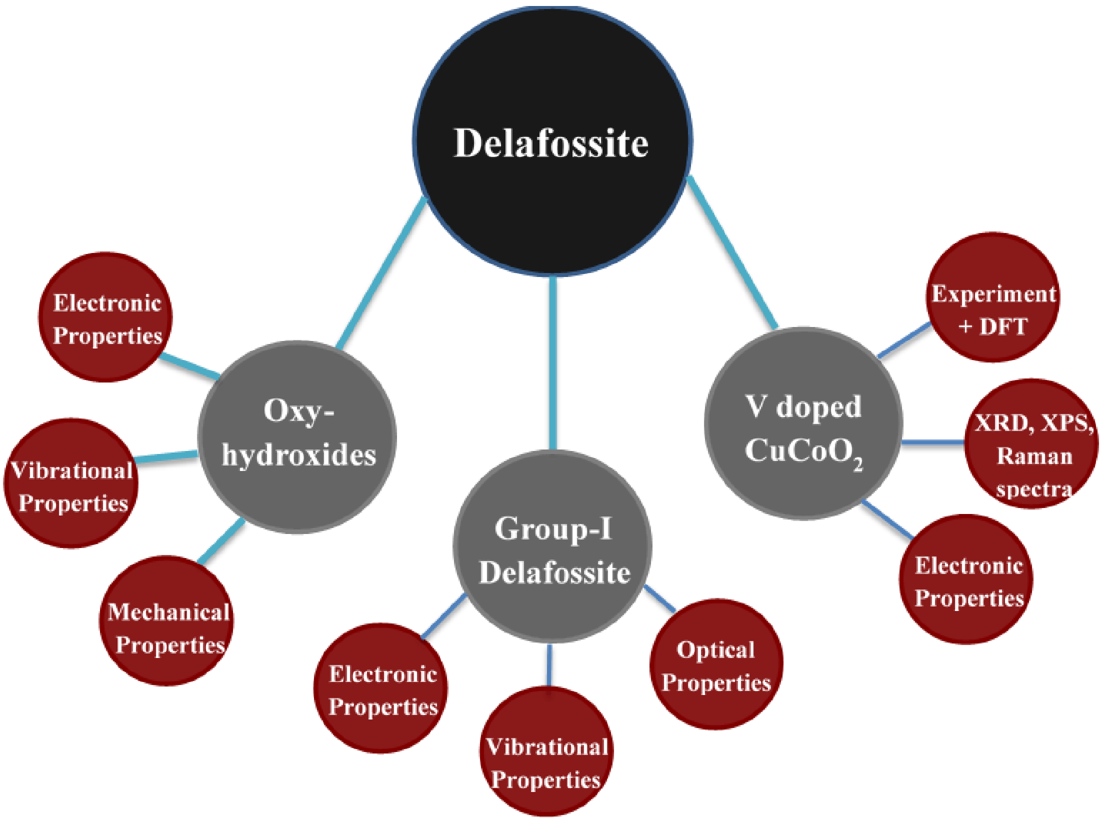

1.1 Overview

Optoelectronic devices that are useful in invisible electronics, functional windows, and dye-sensitized solar cells (DSSCs) are the basic building units of modern technology [1]. Semiconducting oxides are promising family of materials for optoelectronics and electronic devices due to their large electronic and optical band gap. These semiconductors are also useful in energy-conversion devices, photocatalysis, display technology and solar cells. They possess both n-type and p-type conductivities which make them more attractive candidates for transparent conducting oxide (TCOs), photodetectors, and transparent thin-film transistors. Also, these semiconductors show unique ability of being transparent to visible light along with the n/p type conductivity. This unique character of these oxides make them a potential candidate as a transparent material in invisible electronics.

Transparent conducting oxides (TCOs) have been extensively utilized in optoelectronic industries and device applications. The first report on transparent conducting thin films of cadmium oxide (CdO) was published in 1907 by Baedeker [2], who prepared the films by thermal oxidation of sputtered films of cadmium. Since then, extensive works have been done in the field of TCOs technology to prepare new types of TCOs for a wide range of applications [3-6]. These well-known and widely used TCOs are SnO_2, ZnO, In_2O_3, Zn_2SnO_4, $In_4Sn_3O_{12}$, $CdIn_2O_4$, etc. [7-10]. In contrast to the applications, TCOs are extensively used in window layers of solar cells, flat panel displays (FPD), low-emissivity windows, cathode-ray tubes in the video display, smart windows, touch-sensitive control panels, invisible security circuits, gas sensors, organic light-emitting diodes (OLED), etc. Though transparent oxides have a vast range of applications, limited research has been done on device fabrication using TCOs. This is because most of the above mentioned TCOs are n-type semiconductors. However, corresponding p-type transparent conducting oxides (p-TCOs), which are crucial for p-n junction devices, were unexpectedly missing. In 1997, Kawazoe et al. [11] investigated a delafossite type oxide $CuAlO_2$ and reported its p-type semiconducting nature along with the remarkable transparency. The discovery of p-type conductivity and transparency in delafossite $CuAlO_2$ has unlocked a new arena in the field of optoelectronic devices, i.e.,''Transparent Electronics''. The p-type transparent semiconductors combined with the n-type TCOs as p-n junction devices can lead to ''functional devices'' those transmit visible light and generates electricity by absorbing the ultraviolet radiation [11].

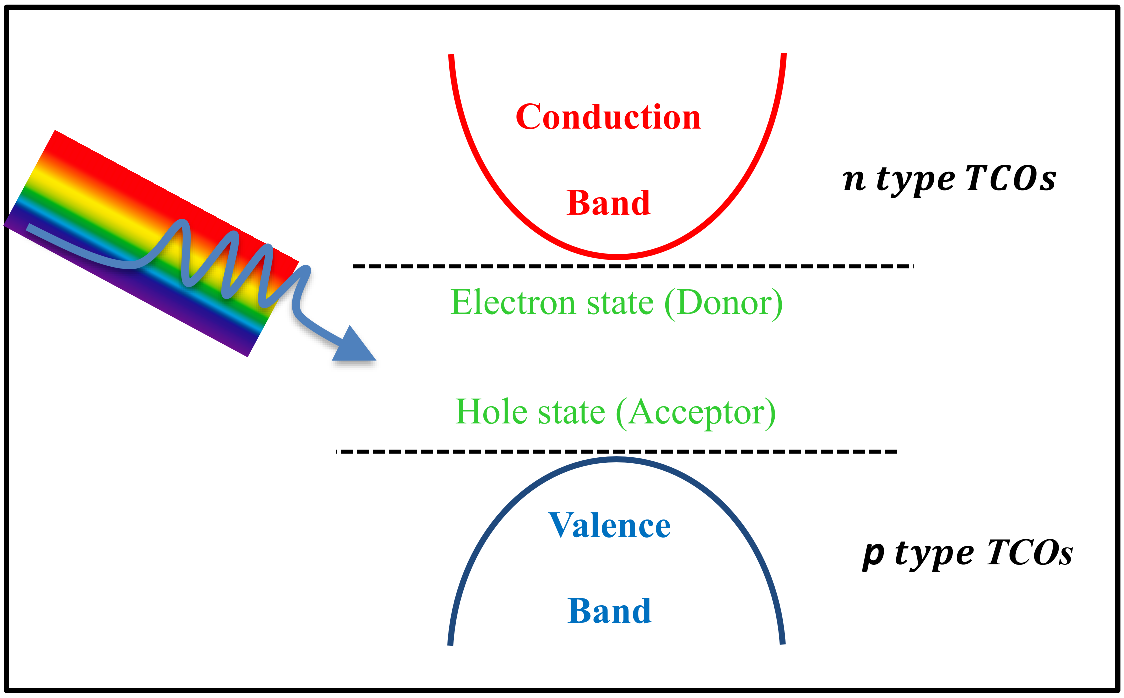

Figure 1.1: The schematic shows the band gap for transparent conducting oxides (TCOs). Incident visible photons induced excited holes and electrons.

The aforementioned novel applications can be possible and it is based on the fact that the electronic band gap of a material used as TCOs is higher than 3.1 eV which corresponds to the energy of wavelength 400 nm. Therefore, the visible light of the energy range between 2.1 to 3.1 eV cannot move electrons from its valence band (VB) to the conduction band (CB) and later are transmitted through it (Fig. 1.1). However, they possess sufficient energy to excite electrons from donor level to CB (for n-type TCOs) or holes from acceptor level to VB (for p-type TCOs).

1.2 p-type Semiconducting Oxides

The existing TCOs are mostly n-type semiconductors while it is principally challenging to design two-fold metal oxides with p-type conductivity due to the electronic structure of these metal oxides [11]. In these metal oxides, the holes are quite localized due to the high electronegative character of oxygen (O). This localization of holes further induced a flat upper valence band in the electronic band structure of these oxides. A deep acceptor level of the holes is generated due to O 2p orbitals because the levels of oxygen are deep compared to the metallic valence orbit [12]. Therefore, the holes are possibly localized around the O atoms and require high energy to cross a barrier height to migrate into the crystal lattice. This localization of holes results in poor conductivity and hole mobility. To overcome these difficulties Kawazoe et al. [11] introduced a ‘‘degree of covalency’’ in the metal-oxygen bindings which introduce the formation of the extended valence band. In other words, the upper valence band is modified by the mixing orbitals of suitable cations that have filled-energy-levels compare to the O 2p level. This valence band engineering is an effective approach to find a good p-TCO. This method is termed as ‘‘Chemical Modulation of the Valence Band (CMVB)’’ [11]. The graphical representation as shown in Fig. 1.2. However, it further requires an appropriate cations. The literature revealed that the essential cations are the $3d^{10}$ closed shell of Cu^+ ions and $4d^{10}$ closed shell of Ag^+ ions [11, 13]. The tetrahedral metal-oxygen coordination is a key to design a better p-TCOs because it reduces the localization of O 2p electrons [11]. In this condition, the valence state of O can be found in sp^3 state. This type of electronic configuration is found in copper oxide (Cu_2O) which is a well-known p-type semiconducting material. The electronic arrangement decreases non-bonding behaviour of O which further delocalizes the holes [14-17]. One of the major limitations of the Cu_2O is its small band gap due to three-dimensional interactions between Cu^+ and $3d^{10}$ electrons [15]. This problem can be solved by utilizing another class of materials known as delafossites, due to their unique structural geometry.

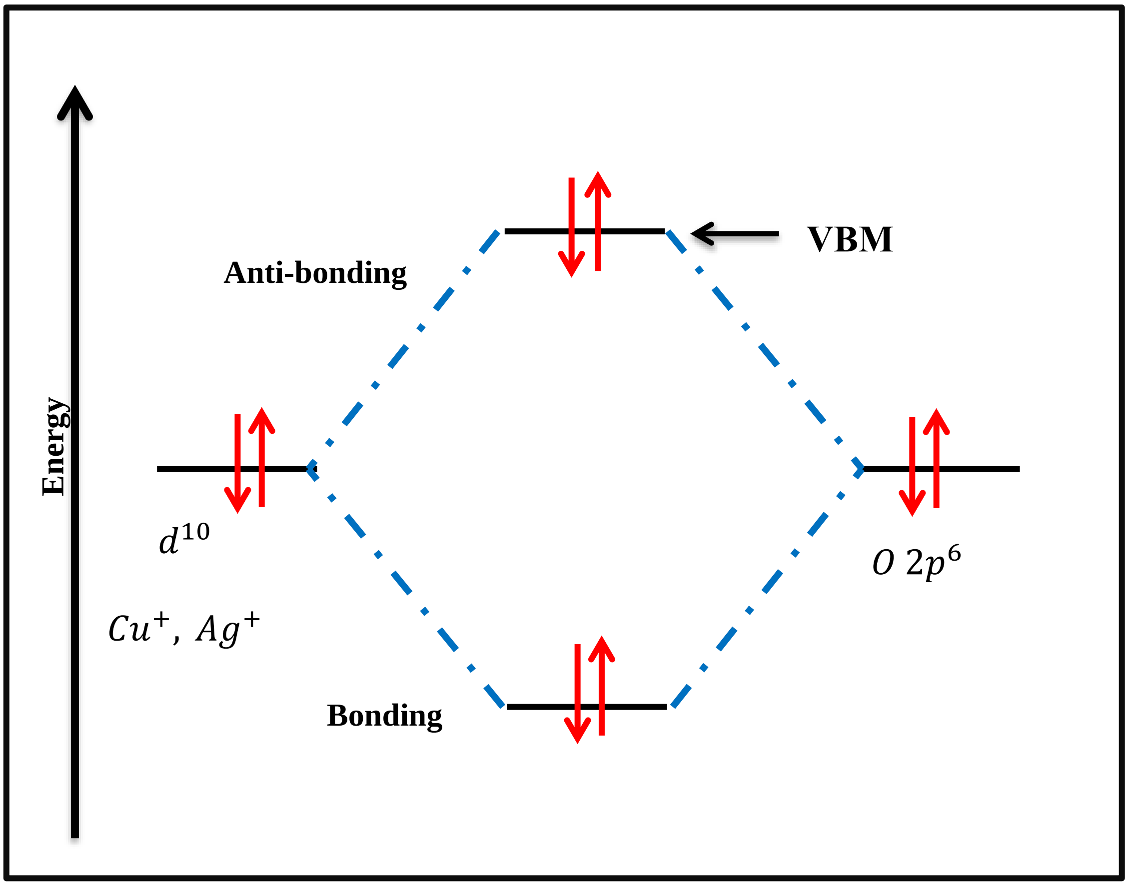

Figure 1.2: Schematic representations of Chemical Modulation of the Valence Band methods.

Materials with delafossite crystal structure with the general chemical formula $A^{+}B^{+3}O_2$ (A= monovalent ions such as Cu^{+1}, Ag^{+1}; B= trivalent ions such as Al^{+3}, Ga^{+3}, In^{+3}, Cr^{+3}, Fe^{+3}, Co^{+3} etc.) have unique characteristics as p-type semiconductor for several reasons [18-20]. The crystal structure of delafossite type compound is shown in Fig. 1.3. It can be seen from Fig. 1.3 that the delafossite structure possesses an alternative layer of A^{+} and layers of nominal $B^{+3}O_2$ composition along with the B^{+3}-O_6 edge sharing octahedra. Each monovalent cation (Cu^{+1}, Ag^{+1}) is linearly connected with two O atoms and makes an O—A^{+1}—O dumbbell shape parallel to the c-axis. Oxygen atoms of O—A^{+1}—O dumbbell links all A^{+1} layers with the $B^{+3}O_2$ layers. In contrast, each O in the $B^{+3}O_2$ layer forms a ‘‘pseudo-tetrahedral coordination ($B^{+3}A^{+1}O$)’’ with the neighbouring B^{+3} and A^{+1} ions [11]. These structural and electronic features reduce the non-bonding character of O and hence delocalize the holes at the upper valence band. On the other hand, layered geometry (O-A^{+1}-O dumbbell layer and $B^{+3}O_2$ layer) effectively reduces the dimension of linkage of metal ions, (A^{+1}) hence enhancing the electronic bandgap [21].

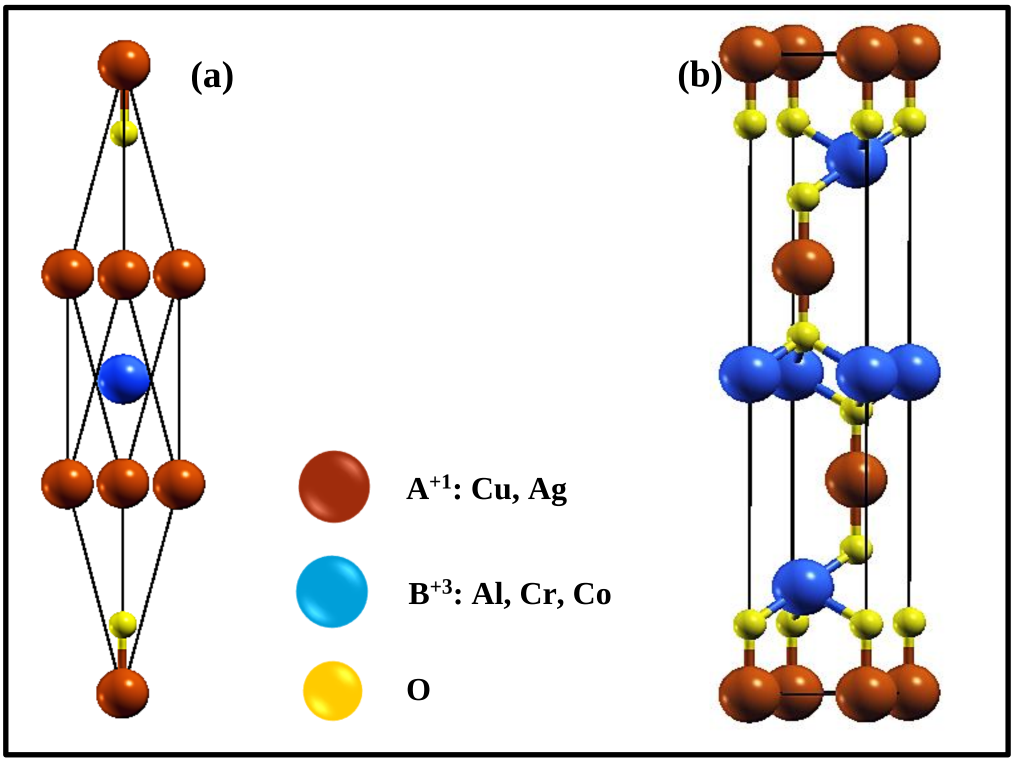

Figure 1.3 : (a) Primitive and (b) conventional cell of delafossite structures.

The low coordination number of the metal ions is another important feature of delafossite structure. The low coordination number originated because of the huge separation from oxygen ligands, which results into the strong Columbic repulsion between O 2p electrons in oxygen ligands and $A^{+1}d^{10}$ electrons. The overlap of metal-oxygen is crucial for good p-type conductivity [21]. For the active device fabrications, it is essential to have lattice matching among both the p- and n-type semiconductors to be used as a p-n homojunction device. The delafossite structure can be suitably applicable for this requirement. It is noteworthy to remark that the $B^{+3}O_2$ layers of delafossite structures are also important to design n-type semiconductors [22].

1.3 Conductivity Limitations and Improvements in Delafossites

Though the delafossite semiconductors exhibit remarkable structural features along with the transparency in the visible region, there are still some challenges in these oxides to be used in practical applications [23-25]. The biggest challenge of these oxides is their low p-type conductivity as compared to the n-type semiconductors which resist them to be used in device applications. The low p-type conductivity originates due to the highly electronegative character of O as well as low metal-oxygen overlap [26]. This further causes the high effective mass of holes. The present development of the oxides in terms of the effective mass of electrons and holes is shown in Fig. 1.4(a).

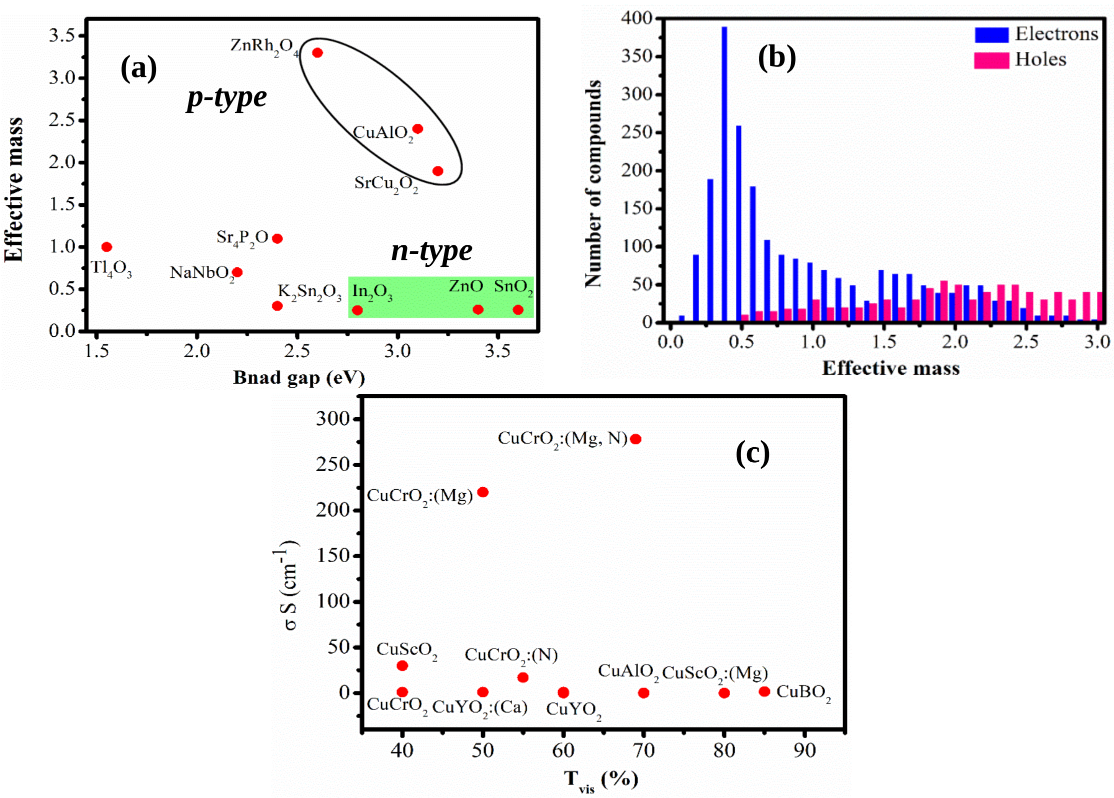

Figure 1.4 : (a) Effective mass versus band gap for the p-type and n-type semiconductors, (b) bar graph shows the effective mass distribution for electrons and holes in oxides, (c) graphical representation of the electrical conductivity (σ) and optical transparency (T_{vis} %) [37] .

It can be seen from Fig. 1.4(a) that the effective mass of holes is very high for p-type semiconductors as compared to the effective mass of electrons in n-type semiconductors. Also, there are less number of available compounds with low hole effective mass (Fig. 1.4(b)). The high hole effective mass also results in the low electrical conductivity in p-type delafossites as compared to the n-type oxides. The highest conductivity is reported for $CuCr_{1-x}Mg_xO_2$ and $CuCr_{1-x}Mg_xN_xO_2$ i.e., 220 Scm^{-1} and 278 Scm^{-1} respectively [27-28]. The conductivity versus transparency of delafossite type oxides is shown in Fig. 1.4(c). In delafossite-type oxides, p-type conductivity is limited mainly due to the low-lying O 2p orbital, while lower hole mobility is caused by the lack of Cu–O–Cu linkages. Meanwhile, the higher conductivity is observed for $CuCrO_2$ and $CuFeO_2$ which may be due to the favourable mixing of monovalent (M^I) and trivalent cations (M^{III}) [29-30]. It is well known that the doping at trivalent metal sites with divalent dopants significantly enhances the conductivity of delafossite-type oxides [31]. Several attempts have been made to explain the trend of increasing conductivity with doping of different divalent cations [29–31]. The conductivity increases due to the reduction in the ionic radius of the M^{III} cations and further decrement in the lattice parameter [32].

There are various methods to enhance the conductivity of these oxides. The most common and effective technique is the doping of transition metal at the place of trivalent cations. Though the transition metal doping enhances the p-type conductivity, but at the same time, it reduces the transparency of these oxides. Therefore, the choice of the dopants is a crucial parameter and one can choose such dopants which increase the band gap as well as the carrier concentrations. In contrast, another method that can help to overcome this limitation is cationic-anionic substitution or co-doping. Recently, this method has gained a lot of attention for delafossite materials. For example, co-doping in the case of $CuAlO_2$ was theoretically investigated using density functional theory (DFT) and produced good results [33]. Further, $CuYO_2$ was synthesized by co-doping of Ca along with rare earth elements [34]. Mg and S doped $CuCrO_2$ have also been explored using this method. Very recently, Ahmadi et al. [28] studied the N and Mg co-doped $CuCrO_2$ and found the record-breaking p-type conductivity. Another effective approach is combining non-conventional elements or trivalent cations with the metal ions [35-36]. In other words, the prediction of new stable delafossite type oxides is the effective approach to get the good p-type semiconductors along with the transparency. On the way of predicting new compounds, the high throughput screening technique is also utilized. Cerqueira et al. [35] investigated 183 different compositions of ABO_2 compounds and established 81 stable compositions. Out of these 81 compounds, some of the new phases are potentially good candidates for transparent electronics. Hautier et al. [37] scanned a large number of compounds to find the best p-type transparent conducting oxides (TCOs) with a low effective mass and a large bandgap. They suggested a few novel earth-abundant, p-type candidates such as BO_6 and $A_2Sn_2O_3$ (A = K and Na) and toxic $PbTiO_3$ and $K_2Pb_2O_3$. The non-oxide delafossite structures are also crucial for achieving good p-type conductivity. Some of them which shows great potential to overcome the conductivity barrier are discussed here.

1.3.1 Chalcogenides and Oxychalcogenides

It has been established that the replacement of O with chalcogen atoms such as S, Se, and Te provides more delocalized holes [38]. These findings boosted the exploration of chalcogen based compounds that possess greater hole mobility as compared to conventional O based delafossites. Very recently, Shi et al. [36] investigated the ternary chalcogenide-based compounds for p-type transparent electrodes and found $AgYS_2$, KYS_2, and $RbYS_2$ with a large bandgap and lower effective mass. Though the chalcogen-based TCOs have greater hole mobility due to their stronger hybridization with Cu 3d states by the chalcogens than O [39], they suffer greatly from their narrow band gap, which limits their visible light transparency [40]. Therefore, it requires an O atom for a large band gap and a chalcogen atom for high hole mobility. Consequently, layered oxychalcogenides have been established to demonstrate a large band gap and high hole mobility due to the hybridization of metal atoms and the chalcogens [41]. Layered oxychalcogenide has alternate layers of transition metals or rare earth elements with O atoms and a metal chalcogen layer, which is important for its p-type conductivity and band gap [42]. The metal chalcogen hybridization forms a direct band gap that allows a direct transition of charge carriers, which is more useful in applications than indirect band gap materials [43-44]. Oxychalcogenides have promising properties that enable them to be used as future transparent p-type materials. For applications such as thin-film transistors (TFTs), which require materials with high mobility, cuprous oxide (Cu_2O) with high hole mobility seems more suitable [45], even though it has a small band gap that is only transparent for part of the visible light range.

1.3.2 Nitride Delafossites

The delafossite structures are not limited to the oxides. Some ABN_2 type nitride materials are also having a great deal of interest to be used as p-type semiconductors. In this context, some unconventional transition metal carbodiimides (MNCN) are also being synthesized and found a great potential as p-type semiconductors for solar cell applications [46-47]. Delafossite structured ternary nitrides, ABN_2 werer also investigated for the applications of tandem solar and photoelectrochemical cells (PECs) [48]. Szymanski et al. [47] investigated nine delafossite-type nitride compounds for their stability, electronic structure, and optical properties. Among them, three of these compounds, $CuTaN_2$, $CuNbN_2$, and $AgTaN_2$ are experimentally synthesised. The $AuTaN_2$ and $AuNbN_2$, have band gaps and absorption onsets near the ideal range for obtaining high solar-cell conversion efficiency, suggesting that these compounds could become potential candidates as absorber materials in tandem solar cells or for band-gap engineering by alloying. Further, Yang et al. [48] studied the electronic and optical properties of $CuTaN_2$ and predicted its applicability as an absorber for solar energy conversion. Cordes et al [49] synthesised the $ATaN_2$ compounds (where A= Na, K, Rb and Cs) and investigated their electronic and optical properties. These compounds can be useful for photovoltaic applications due to their remarkable optical properties.

1.3.3 Oxyhydroxides

It has been recently found that the layered oxyhydroxides are analogous to the ABO_2 type delafossites [50]. In other words, the structural properties of oxyhydroxides and delafossites makes them a potential candidate for optoelectronic applications. The electronic band gap of these materials also shows the potential to be used in photovoltaic and optoelectronic applications. Recently, Burlet et al. [50] found that the natural samples of heterogenite minerals can be characterized as delafossite-type structure, with a general chemical formula ABO_2. By using the spectroscopic techniques, they proved that these oxyhydroxides have a delafossite type structure. Further, the DFT study confirms the 2H ($P6_3/mmc$) and 3R ($R\bar{3}m$) phases of the oxyhydroxide $HCoO_2$ [51]. Very recently, Liu et al. [52] studied the combined $AgCoO_2$ and CoOOH within delafossites (ABO_2) structure. They characterized these structures as alternating layers of A^+ cations and edge-sharing BO_2 octahedra, by mutation of metal oxyhydroxide and delafossite using first-principles calculations. The delafossite type hydroxides can exhibit enhanced oxygen evolution reaction (OER) activity as well as outstanding stability. The combined delafossite and hydroxide structures show a class of promising electrochemical catalysts.

1.3.4 Highly Conductive Metallic Delafossites

The structure of metallic delafossite also contains triangular co-ordinated atomic layers, and electrical transport in the delafossite metals is strongly two dimensional. The most notable feature is their in-plane conductivity, which is amazingly high for oxide metals. At room temperature, the conductivity of non-magnetic $PdCoO_2$ and $PtCoO_2$ is higher per carrier than those of any alkali metal and even the most conductive elements, copper and silver [53]. The delafossite metals, therefore, act like natural heterostructures between strongly correlated and nearly free electron sub-systems. Combined with the extremely high conductivity, they provide many opportunities to study electrical transport and other physical properties in new regimes.

These metallic delafossites are a different class of materials with extreme conductivity and unconventional electron transport. They can be used as superconductors or good electron transport materials due to unconventional electrical conductivity.

1.3.5 Applications of Delafossites

Transparent Electronics and Solar cells: The imminent climate change crisis demands a shift from conventionally used fossil fuels to efficient sources of green energy. This has led researchers to look into the concept of "personalized energy," which would make on-site energy generation possible. For example, solar cells could be integrated into windows, vehicles, cell-phone screens, and other electronic products. But for this, the solar panels need to be handy and transparent [54]. To this end, scientists have developed "transparent photovoltaic" (TPV) devices, transparent versions of the traditional solar cell [55]. The transparent conducting oxides and transparent solar cells have great deals of interest in new technological applications. Unlike the conventionally dark, opaque solar cells which absorb visible light, transparent solar cells make use of the invisible light that falls in the ultraviolet (UV) range. A schematic representation of the aplications of delafossite oxides is presented in Fig. 1.5

Delafossites as Catalysis: The improvement of efficient photocatalysts has been a challenge for the present era. A potential photocatalyst must require extraordinary quantum-efficiency and chemical stability. Families of metal oxides appealed particular attention for their chemical stability in electrolytes [56-64]. However, they are transparent to the solar spectrum and consequently of little practical use. Delafossites possess outstanding longevity, element abundance, much lower cost, and better absorbance in the solar spectrum range. These particular properties make them a potential candidate for photocatalysts [59-62, 64]. However, till date, very few delafossites such as $CuAlO_2$, $CuLaO_2$, $CuCrO_2$, $CuYO_2$, $CuFeO_2$, and $CuRhO_2$ have been reported as photo electrocatalysis [65]. Studies on copper and silver-based delafossites reveal that the visible light absorption of Ag delafossites is lower than copper delafossites due to a larger band gap, although conductivities of silver delafossites are similar or lower. Therefore, there have been tremendous efforts in recent times to improve the photocatalysis activity in delafossites.

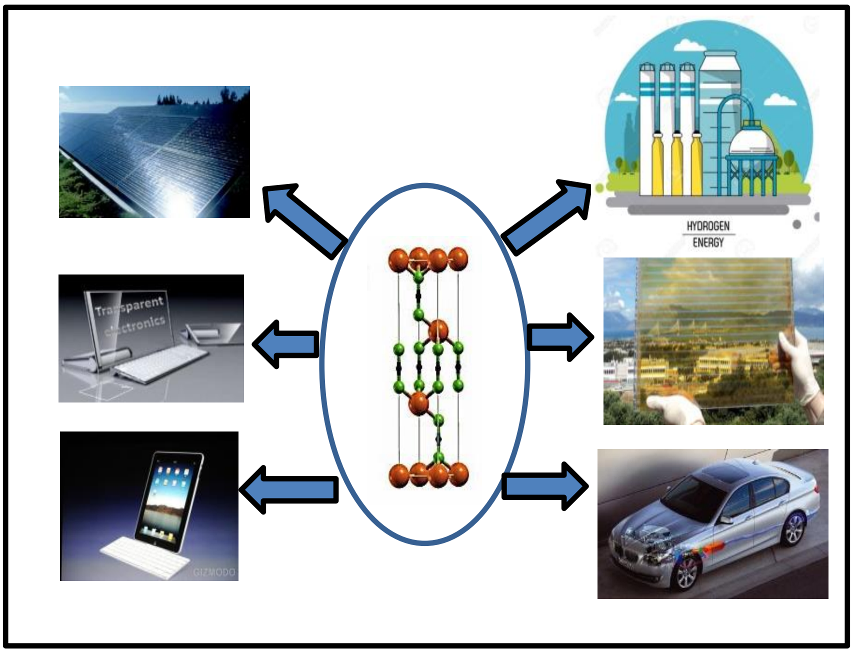

Figure 1.5 : Schematic representations of the applications of delafossite oxides in environmental applications such as catalysis, sensors, and CO_2 reduction, dye sensitized solar cells etc.

Transparent Superconductors: The development of the transparent conductors (TCs) is an important area of research due to their practical as well as fundamental advances [66]. There are variety of materials which have been developed for the TCs applications. For instance, Sn-doped In_2O_3 (ITO) reveals high conductivity (≈6000 Scm^{-1}) and high transparency (~80%) [67]. Likewise, a transparent superconductor (TSC) in the form of $LiTo_2O_4$ films is regarded as an ultimate TC was reported for $LiTi_2O_4$ epitaxial films [68]. Though, the p-type TCs, are subjects of fundamental research, their performances are still low in comparison to n-type TCs [69]. Recently, a new application of the delafossite $CuAlO_2$ is proposed for transparent superconductivity [70]. The delafossite structured $CuAlO_2$ shows the T_c of about 50 K due to a strong electron-phonon interaction and high phonon frequency. These results indicate that the delafossite oxides may be a promising material for fabricating new superconducting materials.

Furthermore, the Fe doped $CuCrO_2$ has been reported for the transparent superconductor with the superconducting transition temperature of 118 K [71].

Gas Sensors: In recent years researchers have found that the transparent conducting oxide (TCO) and its derivatives have proven themselves as one of the most important classes of materials due to having exclusive properties of electrical conductivity and high optical transparency in the visible range [11, 72, 73]. The nanostructured TCOs with controlled structure geometries have attracted extensive interest because these parameters play an important role in determining their optical, electrical, catalytic, and sensing properties [74]. Additionally, these materials also possess new physicochemical properties arising due to their structural geometries [75]. The universality of the toxic gas sensing performance of $CuBO_2$ has attracted extensive interest and attention during the last decade [76]. Recently, $CuCrO_2$ has been applied for room temperature ozone sensors. Delafossites are extensively used for the ammonia gas sensors and a novel p-type delafossite $AgAlO_2$ gas sensor has been reported for ammonia gas sensors. Two dimensional (2D) CoOOH is recently reported for H_2O_2, NH_3, HF, HCN, and H_2S gas sensors [77-78].

Dilute Magnetic Semiconductors: In recent years, many efforts have been made to develop advanced metal oxide semiconductor nanomaterials with exotic magnetic properties for the modern applications [79]. Dilute magnetic semiconductor oxides (DMSOs) are promising candidates for superior control over the charge and spin degrees of freedom. DMSOs are transparent and wide band gap materials with induced ferromagnetism after doping, with a minor percentage of magnetic 3d cation to create a long-range antiferromagnetic order [80]. Significant efforts have been carried out to achieve DMSO with ferromagnetic properties above room temperature. Few metal oxides such as TiO_2, SnO_2, ZnO and In_2O_3 with wide band gap can host a broad range of dopants for the DMSOs applications. Kizaki et al. [81, 82] suggested the delafossite type DMSOs with the transition metal doping. It is established that the Cu, Co and Fe based delafossites are potential candidates for high T_C ferromagnetism with impurity or doping.

1.4 Goal of the Thesis and Objectives

In this thesis, we have investigated the physical properties of newly predicted delafossites as well as the effect of transition metal doping in $CuCoO_2$ delafossite. We have investigated the detailed structural and vibrational properties of 3R ($R\bar{3}m$) and 2H ($P6_3/mmc$) phases of $HCoO_2$. The composition of $HCoO_2$ is different from the conventional delafossites, however, the structure is similar to the delafossite. Our aim is to investigate the structural, electronic, vibrational, and mechanical properties of the $HCoO_2$ compound and to compare these calculated properties with the conventional delafossites. A comparative density functional theory study of the structural, electronic, vibrational, and optical properties of group I based delafossite $CuMO_2$ (M = H, Li, Na, K, Rb) is performed. The present work is also focused on the idea of the exploration of new structural features of delafossite-type oxides with a combination of alkali metals. It is well established that the doping of transition metal ions at the place of trivalent cations results in high electrical conductivity and low hole effective mass. Here, $CuCo_{1-x}V_xO_2$ is explored for the structural, electronic, and magnetic properties.

1.5 Organization of Dissertation

The rest of the dissertation is organized as follows: In **Chapter 2**, the the density functional theory and the experimental techniques for sample preparation are briefly described. Computational details of the vibrational and optical properties are also described in this chapter. Furthermore, the characterization techniques such as X-ray diffraction, Raman Spectra, X-ray photoemission (XPS), Vibrating Sample Magnetometer (VSM) are discussed. The challenges of the electronic band structure and phonon calculations for the complexes are explained.

In **Chapter 3**, the structural, electronic, vibrational and mechanical properties of hexagonal (2H) and rhombohedral (3R) phases of $HCoO_2$ are described. The high-pressure behaviour of both polytypes of $HCoO_2$ is determined using state of the art first principles calculations based on DFT. The details of different exchange correlation functionals such as local density approximation (LDA) and generalized gradient approximation (GGA) and their effects on electronic properties are discussed. The structural properties of both polytypes of $HCoO_2$ are investigated in this chapter. Here, we have explored the structure, electronic and vibrational properties of both the polytypes and compare these properties with the conventional delafossite. Further, the high pressure behaviour of both polytypes of $HCoO_2$ is investigated. For the accurate description of electronic band gap we have used different approximation such as LDA and GGA. Additionally, the electronic band structure is calculated using the on-site coulomb interaction U term. These two polytypes exhibits indirect band gap semiconductors with the band gap in the range of 2.01 eV-2.06 eV. Further, the structural evolution with respect to the pressure depicted the change in lattice parameters, volume and the bond length of these polytypes. The linear decrement in O-H bond length with pressure is observed for both phases with pressure. The phonon dispersion curves show the dynamical instability of 2H phase at 35 GPa while the 3R phase is unstable around 40 GPa. Raman spectra show that the A_{1g} mode is more sensitive to the pressure. The mechanical stability of these compounds investigated in terms of the stiffness matrix and Born stability criteria. The elastic constants of 2H- and 3R-$HCoO_2$ shows the existence of phase transition beginning around 34.3 and 38.3 GPa pressure derived from the shear modulus. The results reported in this chapter have appeared in the following publication:

- D. Upadhyay, A. Pratap, P. K. Jha "A first principles study on structural, dynamical and mechanical stability of newly predicted delafossite $HCoO_2$ at high pressure" *J. Raman Spectrosc.* **50** (2019) 603-613.

In **Chapter 4**, a comparative study of the structural, electronic, vibrational and optical properties of the alkali atom based $CuMO_2$ (M= H, Li, Na, K, Rb) is reported. The description of electronic band structure along with the projected density of states (PDOS) is presented in terms of hybridization of the orbitals. Finally, the applicability of these compounds is discussed with respect to the optoelectronics applications. Although the similar chemical compositions of group I based delafossites ($CuMO_2$ (M = H, Li, Na, K, and Rb)), display diverse structural, electronic, dynamical, and optical properties. The atomic radii of the different elements of group I, starting from H to Rb has significant influence in their electronic, lattice dynamical and optical properties. We determine the uniqueness of ground state properties of these compounds by means of first principle calculations based on the density functional theory (DFT). The electronic band structures, phonon dispersion curves (PDCs) and the optical properties are profoundly linked with the atomic radii of the group-I atoms. The electronic band gap of $CuMO_2$ (M = H, Li, Na, K, and Rb) found within the range of 0.5-1.0 eV, categorized them in the low band gap p-type semiconductors. The band gap increase with respect to the atomic radii of the alkali atoms like the conventional delafossites. The metal-oxygen (Cu-O) overlap is observed due to the robust p-d hybridization. Dynamical stability is confirmed from the phonon dispersion curves, as there is no imaginary frequency observed in the entire Brillouin zone. The refractive index and static dielectric constants fall within the range of 1.98-3.55 and 8.0-12.91 respectively, suggesting the utility in none-linear optical devices. The optical properties depicted the utility of these delafossites as promising candidates for improved optical devices. The findings of this chapter have appeared in the following publication:

- D. Upadhyay, N. Joshi A. Pratap, P. K. Jha "Comparative ab initio study of the structural, electronic, dynamical, and optical properties of group-I based $CuMO_2$ (M = H, Li, Na, K, Rb)" *J. Appl. Phys*. 128 (2020) 155701.

In **Chapter 5**, the effects of vanadium doping on the structural, electronic and magnetic properties of $CuCoO_2$ are described. The method of sample preparation, characterization techniques, and the brief description of the computational parameters are provided in this chapter. The XRD diffraction patterns confirm pure rhombohedral phase formations of pristine CCO and V doped CCO. The V prefers the tetravalent occupancy (V^{+4}) when doped at Co site. The VBM modulation is observed during V doping due to higher metal oxygen overlap. The pristine CCO compound shows an indirect band gap of 1.03 eV while it reduced to 0.40 eV when doped with V atoms. Furthermore, we report a study of magnetic properties of delafossite CCO and CCVO by a vibrating sample magnetometer (VSM). The pristine CCO and doped CCVO compounds shows paramagnetic behavior. The V doping slightly increases the magnetization values confirmed by the theoretical calculations. The magnetic properties of these compounds are also depends on ionic radii of trivalent atoms. The electronic band structure and the PDOS of these compounds indicated the p-d hybridizations induced by the V doping. The p-d hybridizations observed in V doped CCO indicated that the substitution of V at the Co site generates more free holes and it is good for better p-type conductivity. The results of dielectric constant and absorption coefficient of pristine and V doped CCO indicate that these compounds can be used in optoelectronics. Refractive index spectra increase in the visible region and the reflectivity spectra show maximum peaks in the ultraviolet region, and the loss spectra indicate the least energy loss by an electron in the visible region, confirming potential applications of these compounds in optoelectronic applications. The findings of these studies have appeared in the following work:

- D. Upadhyay, A. Pratap, P. K. Jha "Effects of vanadium doping on the structural and electronic properties of $CuCoO_2$" *(In Communication).*

In **Chapter 6**, summary of the present thesis, overall output and applicability of these findings are discussed. The future scope is also discussed in this chapter.

References

1. A. N. Banerjee and K. K. Chattopadhyay, *Prog. Cryst. Growth Charact. Mater.* **50**, 52 (2005).
2. K. Baedeker, *Ann. Phys*. (Leipzig) **22**, 749 (1907).
3. R. G. Gordon, *MRS Bull.* **25**, 52 (2000).
4. J.M. Philips, R.J. Cava, G.A. Thomas, S.A. Carter, J. Kwo, T. Siegrist, J.J. Krajewski, J.H. Marshall, W.F. Peck Jr., D.H. Rapkine, *Appl. Phys. Lett*. **67**, 2246 (1995).
5. C. J. Petti, M. M. Hilali, G. Prabhu, Handbook of Thin Film Deposition (Third Edition), (2012).
6. Z. B. Wang, M. G. Helander Z. H. Lu Woodhead Publishing Series in Electronic and Optical Material, 49-76 (2013).
7. K. Al-Attafi, F. H. Jawdat, H. Qutanish, P. Hayes, A. Al-Keisy, K. Shim, Y. Yamauchi, S. X. Dou, A. Nattestad, J. H. Kim, *Nano Energy*, **57**, 202 (2019)
8. A.N. Banerjee, S. Kundoo, P. Saha, K.K. Chattopadhyay, *J. SoleGel Sci. Technol*. **28**, 105 (2003).
9. J. Hu, R.G. Gordon, *J. Appl. Phys*.**72**, 5381 (1992).
10. A. N. Banerjee, R. Maity, S. Kundoo, K. K. Chattopadhyay, *Phys. Status Solidi A.* **201**, 983 (2004).
11. H. Kawazoe, M. Yasukawa, H. Hyodo, M. Kurita, H. Yanagi, H. Hosono, *Nature.* **389**, 939 (1997).
12. S. Fraga, S. Karwowski, K.M.S. Saxena, Handbook of Atomic Data, Elsevier, Amsterdam (1976).
13. D. DeVault, *J. Chem. Educ*. **21**, 526 (1944).
14. Y. K. Leung, A. K. Khan, J. F. Kos, F. P. Koffyberg, Procee. Nat. Conf. Solar Energy, Solar Energy Society of Canada, Montreal, 124 (1981).
15. J. P. Dahl, A. C. Switendick, *J. Phys. Chem. Solids.* **27**, 931 (1966).
16. M. Hayashi, K. Katsuki, *J. Phys. Soc. Jpn*. **5**, 380 (1950).
17. L. Kleinman, K. Mednick, *Phys. Rev. B.* **21**, 1549 (1980).
18. R.D. Shannon, D.B. Rogers, C.T. Prewitt, *Inorg. Chem*. **10**, 713 (1971).
19. C.T. Prewitt, R.D. Shannon, D.B. Rogers, *Inorg. Chem*. **10**, 719 (1971).
20. D.B. Rogers, R.D. Shannon, C.T. Prewitt, J.L. Gilson, *Inorg. Chem.* **10**, 723 (1971).
21. H. Kawazoe, H. Yanagi, K. Ueda, H. Hosono, *MRS Bull.* **25**, 28 (2000).

22. T. Otabe, K. Ueda, A. Kudoh, H. Hosono, H. Kawazoe, *Appl. Phys. Lett*. **72**, 1036 (1998).
23. E. Fortunato, P. Barquinha, and R. Martins, *Adv. Mater*. **24**, 2945 (2012).
24. D. O. Scanlon, G. W. Watson, *J. Phys. Chem. Lett*. **21**, 3195 (2010).
25. B. Williamson, J. Buckeridge, B. Jennilee, S. Ansbro, R. G. Palgrave, D, O. Scanlon, *Chem. Mater*. **29**, 2402 (2017).
26. R. Nagarajan, A. D. Draeseke, A. Sleight, J. Tate, J. *Appl. Phys*. **89**, 8022 (2001).
27. J. F. H. L. Monteiro, A. R. Jurelo, E. C. Siqueria, *Solid state commun.* **252**, 64 (2017).
28. M. Ahmadi, M. Asemi, M. Ghanaatshoar, *Appl. Phys. Lett*. **113**, 242101 (2018).
29. R.G. Gordon, U.S. Patent No. 4, 146, 657, (1979).
30. A.N. Banerjee, S. Kundoo, P. Saha, K. K. Chattopadhyay, *J. Sol. Gel Sci. Technol*. **28,** 105 (2003).
31. A.N. Banerjee, R. Maity, S. Kundoo, K. K. Chattopadhyay, *Phys. Status Solidi*. **201**, 983, (2004).
32. S. Major, A. Banerjee, K.L. Chopra, *Thin Solid Films*. **122**, 31 (1984).
33. Q.-J. Liu, H. Qin, Z.-T. Liu, *Commun. Theor. Phys*. **65**, 527 (2016).
34. N. Tsuboi, T. Hoshino, S. Kobayashi, K. Kato, F. Kaneko, *Phys. Status Solidi*. **203**, 2723 (2006).
35. T. F. Cerqueira, S. Lin, M. Amsler, S. Goedecker, S. Botti, M. A. L. Marques, *Chem. Mater*. **27**, 4562 (2015).
36. J. Shi, T. F. T. Cerqueira, W. Cui, F. Nogueira, S. Botti, M. A. L. Marques, *Sci. Rep*. **7**, 43179 (2017).
37. G. Hautier, A. Miglio, G. Ceder, G. M. Rignanese, X. Gonze, *Nat. Commun*. **4**, 2292 (2013).
38. N. Joshi, D. Upadhyay, A. Pandya, P. K. Jha, *J. Appl. Phys*. **126**, 235705 (2019).
39. M. L. Liu, L. B. Wu, F. Q. Huang, L. D. Chen, J.A Ibers, *Solid. State. Chem*. **180**, 62 (2007).
40. A. Kudo, H. Yanagi, H. Hosono, H. Kawazoe, *Appl. Phys. Lett*. **73**, 220 (1998).
41. N. Zhang, J. Sun, H. Gong, *Coatings*. **9**, 137 (2019).
42. K. Ueda, H. Hiramatsu, M. Hirano, T. Kamiya H. Hosono, *Thin Solid Films*. **496**, 8 (2006).
43. K. Ueda, H. Hosono, N. Hamada, *J. Appl. Phys*. **98**, 043506 (2005).
44. K. Ueda, S. Inoue, H. Hosono, N. Sarukura, M. Hirano, *Appl. Phys. Lett*. **78**, 2333 (2001).

45. J. P. Hu, D. J. Payne, R. G. Egdell, P. A. Glans, T. Learmonth, K. E. Smith, J. Guo, N. M. Harrison, *Phys. Rev. B*. **77**, 155115 (2008).
46. T. Jiang, B. Polteau, Y. Farre, L. Cario, C. Latouche,Y. Pellegrin, M. Boujtita, F. Odobel, F. Tessier, F. Chevire¸ S. Jobic, *Inorg. Chem*. **56**, 7922 (2017).
47. N. J. Szymanski, L. N. Walters, O. Hellman, D. Gall S. V. Khare, *J. Mater. Chem. A*. **6**, 20852 (2018).
48. M. Yang, A. Zakutayev, J. Vidal, X. Zhang, D. S. Ginley, Francis J. DiSalvo, *Energy Environ.* Sci. **6**, 2994 (2013).
49. N. Cordes, R. Niklaus, W. Schnick, *Cryst. Growth Des*. **19**, 3484 (2019).
50. C. Burlet, H. Goethals, Y. Vanbrabant, *Spectrochim. Acta A Mol. Biomol. Spectrosc*. **159**, 90 (2016).
51. D. Upadhyay, A. Pratap, P. K. Jha, *J. Raman Spectrosc*. **50**, 603 (2019).
52. J. Liu, Q. Hu, Y. Wang, Z. Yang, X. Fan, L.M. Liu, L. Guo, *Proc. Natl. Acad. Sci. U.S.A.* **117**, 36, (2020).
53. A. P. Mackenzie, *Rep. Prog. Phys*. **80**, 032501 (2017).
54. A. A. F. Husaina, W. Zuha, W. Hasana, S. Shafiea, N. Hamidonb, S. S. Pandey, *Renew Sustain Energy Rev*. **94**, 779 (2018).
55. C. J. Traverse, R. Pandey, M. C. Barr, R. R. Lunt, *Nat. Energy*. **2**, 849 (2017).
56. C. Mondelli, A. P. Amrute, T. Schmidt, J. Pérez-Ramírez, *Chem. Comm*. **47**, 7173 (2011).
57. S. Y. Choi, C.-D. Kim, D. S. Han, H. Park, *J. Mater. Chem. A.* **5**, 10165 (2017).
58. N. Koriche, A. Bouguelia, A. Aider, M. Trari, *Int. J. Hydrogen Energy*. **30**, 693 (2005).
59. N. Koriche, A. Bouguelia, M. Trari, *Int. J. Hydrogen Energy*. **31**, 1196 (2006).
60. Q.-M. Zhao, Z.-Y. Zhao, Q.-L. Liu, G.-Y. Yao, X.-D. Dong, *J. Phys. D Appl. Phys*. **53**, 135102 (2020).
61. S. Saadi, A. Bouguelia, A. Derbal, and M. Trari, *J. Photochem. Photobio. A Chem*. **187**, 97 (2007).
62. S. Santra, N. S. Das, and K. K. Chattopadhyay, *Materi. Res. Bullet*. **48**, 2669 (2013).
63. S. Kato, N. Takagi, K. Saito, and M. Ogasawara, *ACS Omega*. **4**, 9763 (2019).
64. Y. Maruyama, H. Irie, and K. Hashimoto, *J. Phys. Chem. B*. **110**, 23274 (2006).
65. J. E. Park, Y. Hu, J. W. Krizan, Q. D. Gibson, U. T. Tayvah, A. Selloni, R. J. Cava, A. B. Bocarsly, *Chem. Mater*. **30**, 2574 (2018).
66. D. S. Ginley, C. Bright, *MRS Bull.* **25,** 8 (2011).

67. H. Ohta, M. Orita, M. Hirano, H. Tanji, H. Kawazoe, H. Hosono, *Appl. Phys. Lett*. **76**, 2740 (2000).
68. A. Kumatani, T. Ohsawa, R. Shimizu, Y. Takagi, S. Shiraki, T. Hitosugi, *Appl. Phys. Lett.* **101**, 123103 (2012).
69. K. H. L. Zhang, K. Xi, M. G. Blamire, R. G. Egdell, *J. Phys. Condens. Matter*. **28**, 383002 (2016).
70. E. R. Ylvisaker, W. E. Pickett, *Phys. Rev. B*. **74**, 075104 (2006).
71. C.Taddee, T. Kamwanna, V. Amornkitbamrung, *Appl. Surf.* Sci. **380**, 237 (2016).
72. C.S. William, E. Mugnier, A. Barnabe, J.M. Tobin, R.P. Kenneth, *Chem. Mater*. **18**, 7 (2006).
73. G. Thomas, *Nature*. **389**, 907 (1997).
74. S. Thirumalairjan, K. Girija, V.R. Mastealro, N. Ponpandian, *ACS Appl. Mater. Interfaces*. **6**, 13917 (2014).
75. H.M. Luo, M. Jain, T.M. McCleskey, E. Bauer, A.K. Burrell, Q.X. Jia, *Adv. Mater*. **19,** 3604 (2007).
76. H. Yanagi, S. Inoue, K. Ueda, H. Kawazoe, H. Hosono, N. Hamada, *J. Appl. Phys*. **88**, 4159 (2000).
77. D. Upadhyay, B. Roondhe, A. Pratap, P K. Jha, *Appl. Surf.* Sci. **476**, 198 (2019).
78. F. Opoku, P. P Govender, *Electroanal*. **32**, 2764 (2020).
79. T. A. Dietl, *Nat. Mater*. **9**, 965 (2010).
80. A. Gupta, R. Zhang, P. Kumar, V. Kumar, A. Kumar, *Magnetochemistry*. **6**, 15 (2020).
81. H. Kizaki, K. Sato, H. Katayama-Yoshida, *AIP Conf Proc*. **401**, 462 (2007).
82. H. Kizaki, K. Sato, H. Katayama-Yoshida, *Jpn. J. Appl. Phys*. **47**, 6488 (2008).